

# Modeling of Activated Sludge Transient Behavior Induced by Regulation of Carbon and Nitrogen Metabolism

B. Lavallée

Direction des Politiques de l'eau, Ministère du développement durable, de l'Environnement et des Parcs, Gouvernement du Québec, Canada, G1R 5V7

P. Lessard and P. A. Vanrolleghem

Département de génie civil et de génie des eaux, 1065 av. de la Médecine, Université Laval, Québec, Canada, G1V 0A6

DOI 10.1002/btpr.683

Published online September 13, 2011 in Wiley Online Library (wileyonlinelibrary.com).

*An experimental protocol to evaluate the structured biomass model proposed by Lavallée (Lavallée, Lessard, and Vanrolleghem, J Environ Eng Sci 2005;4:517–532) is presented. The protocol was devised to induce transient behavior and characterize the evolution of several internal biomass components. The proposed model is based on biochemical principles, and was fitted to the collected data. In these experiments, it was observed that filling the storage capacity of cells leads to special transient behavior, including a temporarily reduced metabolic activity. The model-based interpretation of the results showed that the observed transient behavior can be explained by cross-regulation of carbon and nitrogen metabolism. Hence, according to an extensive literature review, the cross-regulation of carbon and nitrogen can be used to model some observed transient behaviors and regulation of the storage process in activated sludge. © 2011 American Institute of Chemical Engineers Biotechnol. Prog., 27: 1522–1534, 2011*

*Keywords: accumulation capacity, activated sludge, mathematical modelling, metabolic model, nitrogen regulation, structured biomass model, transient behavior*

## Introduction

Increasingly, RNA-based molecular techniques are used in wastewater treatment process monitoring and microbial ecology studies.<sup>1</sup> The quantification of active cells by the use of probes thus allows the development of refined models regarding the description of active biomass because the variation of their specific activity can then be taken into account.<sup>2</sup> In fact, using these techniques, Hao<sup>3</sup> showed that activity decay contributed to the decreased activity of ordinary heterotrophic organisms, ammonium, and nitrite oxidizing bacteria. Such models would help in understanding the transient behavior of the activated sludge process and in the design and the operational optimization of the process. With such a structured biomass model, it should also be possible to find the intrinsic value of parameters<sup>4</sup> defining the growth rate of the biomass on a given substrate. Based on an extensive literature review,<sup>5</sup> Lavallée<sup>6</sup> proposed a structured biomass model including peripheral enzymes and ribosome (or rRNA-level) regulation to model fluctuations of the maximal growth rate and the resulting transient behavior of mixed cells cultures.

Among several types of transients observed in activated sludge, it was observed that filling the cell's accumulation capacity leads to a decrease of its metabolic activity.<sup>7</sup> When cells are exposed to high substrate concentrations, Chang<sup>8</sup>

observed that cells appear to exhibit saturation of their anabolic fluxes, suggesting a kinetic limitation for precursor metabolite production downstream of the carbon incorporation into cell mass. These authors observed also that poly- $\beta$ -hydroxybutyrate (PHB) production could restore the balance between metabolic fluxes.

Aon<sup>9</sup> observed that under various C:N ratios, *Saccharomyces cerevisiae* appear to exhibit a saturation of anabolic fluxes and observed that an imbalance between metabolic fluxes induces ethanol production when any nutrients but carbon were limiting for growth. According to these authors, a slow incorporation rate of nitrogen limits the glutamate synthesis and induces an oversupply of precursors as  $\alpha$ -ketoglutarate and metabolites of the tricarboxylic acid cycle (TCA cycle).

In the literature, pathways of carbon and nitrogen metabolism are well described. Glutamate and glutamine are the key nitrogen donors for biosynthetic reactions.<sup>10</sup> Hence, the carbon assimilation into cell constituents is linked to nitrogen incorporation through the TCA cycle and glutamate synthesis. When organic substrate and nitrogen are available in high concentrations, a high carbon consumption rate is observed, and the lower rate of nitrogen supply induces a limitation in anabolism. Afterward, the high substrate uptake rate and the lower rate of anabolism can be balanced by fermentation or storage processes. Such conditions can be found in SBR and in EBPR processes where substrate is fed in batch to promote glycogen, PHB, or polyphosphate accumulation.

Correspondence concerning this article should be addressed to B. Lavallée at Bernard.Lavallee@mddep.gouv.qc.ca.

Given current knowledge, induction and regulation of the carbon uptake and storage by C/N imbalance in cells seems well understood from a biochemical point of view in pure culture.<sup>8–10</sup> However, no model has yet been suggested to describe the behavior of activated sludge cells under such conditions. Hence, in this work, the hypothesis that the induction of the storage process and the substrate uptake rate can be regulated by a saturation of anabolic fluxes was tested by modeling observed transient behavior of mixed cultures of cells.

A new structured biomass model is thus proposed in this paper; it is based on the Lavallée<sup>6</sup> model and on biochemical regulation principles proposed for single species in aerobic processes. The aim of the model is to simulate transient behavior induced in semi-batch and batch reactors. A transient that got particular attention was the unexpected reduced metabolic activity observed after substrate oversupply. Unbalanced uptake rates of carbon and nitrogen were suspected to induce a saturation of the anabolic flux. The transients were modeled using the cross-regulation pattern of carbon and nitrogen metabolism proposed in the literature for pure cultures of bacteria. Also proposed is an experimental protocol to validate the underlying assumptions and support the calibration of such a model.

## Material and Methods

### Experiments

The mixed culture was grown in a semi-continuous reactor for adaptation of biomass and preliminary testing for a period of more than 24 months. The reactor was inoculated with sludge from a municipal SBR wastewater treatment plant located in Lévis (QC, Canada). The culture was maintained in suspension with a mechanical mixer running at  $\pm 60$  rpm, and the dissolved oxygen concentration was close to 8 mg/L with porous diffusers. The reactor volume was 3.25 L and the hydraulic and sludge residence time was close to 6 days. The TSS in the reactor was close to 800 mg COD/L and the mixed liquor overflowed to the effluent.

Substrate was added within 3 minutes every 3 hours. The substrate used was made of glucose (4.5 g),  $\text{NH}_4\text{Cl}$  (0.91 g),  $\text{KH}_2\text{PO}_4$  (7.47 g),  $\text{KH}_2\text{PO}_4$  (1.435 g),  $\text{MgSO}_4 \cdot 7\text{H}_2\text{O}$  (1.095 g), 12 mL of trace elements solution<sup>11</sup> and distilled water (completion to 3 L). Nitrification was inhibited in the reactor by periodically adding allylthiourea doses of 100 mg/L.<sup>12</sup> Inhibition of nitrification was required to perform ammonia balances and nitrogen consumption by growing biomass. The phosphate buffer maintained the pH of the mixed liquor close to  $6.9 \pm 0.1$ . Growth of protozoa was inhibited by applying an anaerobic period of 3 hours daily.<sup>13</sup> In one culture, growth of protozoa was inhibited by adding cycloheximide (0.6 g) and colchicine (0.3 g) to the substrate solution.<sup>14</sup> However, microscopic observations showed that the inhibition was only efficient during a limited period of time and regrowth of protozoa was observed in both experiments.

To perform a validation of the model under different experimental conditions, an initial  $S_0/X_0$  ratio of 9.9 was first used in a batch experiment to ensure exponential growth, and in a subsequent experiment,  $S_0/X_0$  ratios of 1.5, 1.5, and 2.2 in three consecutive substrate pulses were used. For these two batch experiments, 1.5 and 0.5 L of mixed liquor volume of 100 and 350 mg COD/L TSS, respectively, was

taken from the semi-continuous reactor and mixed with the substrate solution. Glucose and nitrogen quantities were adjusted to the required concentrations and glucose was added at time zero in the exponential growth experiment and at time 1.50, 4.20, 5.25 hours, respectively, in the three pulses experiment. As in the semi-continuous reactor, the biomass was maintained in suspension with a mechanical mixer and the dissolved oxygen concentration was maintained close to 8 mg/L. The temperature of all reactors was regulated at  $20.0 \pm 0.1^\circ\text{C}$ .

The exponential growth batch experiment was conducted four times using various glucose substrates and proved the observed transient behavior to be reproducible. The three pulse experiment was conducted twice and the oxygen uptake rate pattern was the same in both. Hence, it was concluded that the observed transient behaviors were repeatable and were not induced by some unknown inhibitor.

### Analysis

The active biomass concentration ( $X_H$ ) was quantified by DNA analysis which was chosen as an arbitrary unit for cell number. The assumption was that the ratio of cell structure (surface of cell wall) per nucleus remains constant and independent of growth rate.<sup>15</sup> This unit of cell wall membrane bound proteins and nucleus was used as a basic unit of the cell's structure. Hence, the COD of the cell's structure ( $X_H$ ) was evaluated using a constant  $X_H/\text{DNA}$  ratio (mg of COD/ $\mu\text{g}$  of DNA). Using this assumption, it was then possible to assess the mass of pool material, similar to Schaechter.<sup>15</sup>

Aliquots were taken in four replicates, and EDTA was added to inhibit DNase<sup>16</sup> and norfloxacin and Katlon® was added to inhibit DNA gyrase.<sup>17</sup> The stabilized samples were stored at  $4^\circ\text{C}$  until DNA was extracted and quantified in each replicate. Exogenous DNA was extracted using Crown-ether<sup>18</sup> before cell lysis. Then, the replicates were centrifuged at 16,000g during 10 minutes at  $4^\circ\text{C}$ . For cell lysis, the pellets were bead-beated continuously during 5 minutes at 4,800 cycles/minute in a 3% SDS solution. The SDS extraction of DNA, ammonium acetate purification, and ethanol precipitation was performed according to Yu.<sup>19</sup> DNA quantification was performed by fluorescence using the Hoescht 33258 fluorochrome.<sup>20</sup> Fluorescence was measured using a Sequoia-Turner model 450 fluorometer, and filters of 360 and 450 nm. The full width-half maximum of the band-pass was  $\pm 10$  nm and the precision of the central wavelength was  $\pm 2$  nm. The DNA concentration was obtained from a calibration curve constructed with pure calf thymus DNA (Sigma DNA standard D.4810). The confidence interval of the standard curve varied between 1 and 4 ng DNA/mL for low and high DNA concentrations, respectively. The extraction and purification method were applied to pure DNA aliquots. The percentage of DNA recovery was only 37% but the method remained linear for various aliquot volumes. The detection limit of the method applied to biomass was 45 ng DNA/mL. The standard deviation of the extracted DNA varied between 10 and 20% of the replicate's mean.

The total COD and soluble COD were measured by using the closed reflux and titration method described in Standard Methods.<sup>21</sup> Analyses were done in triplicate. Commercially prepared 1500 COD Hach™ tubes were used. For soluble COD measurements, samples were filtered on superposed fibre glass 934 AH filters and 0.45  $\mu\text{m}$  polycarbonate HTPP

filters of Millipore. The standard deviation of total and soluble COD triplicates was less than 1% of the mean. The particulate COD was obtained by subtracting the soluble COD from the total COD value.

The Nessler method was used for  $\text{NH}_4^+$  measurement on filtered samples.<sup>21</sup> Hach™ commercially prepared solutions were used. The filtration method was the same as for COD. The method was adapted to 3-mL samples and measurements were performed directly in polymethacrylate dishes after dilution, and read at 425 nm. The standard deviation of triplicates was always lower than 0.7 mg/L.

Soluble carbohydrates (e.g., glucose) and particulate carbohydrates (e.g., glycogen) were measured using the anthrone method.<sup>22,23</sup> Filtered samples were stored at 4°C in sterilized vials until analysis. The filtration method was as used for COD. A few drops of formaldehyde were added to unfiltered aliquots to inhibit glycogen metabolism.<sup>12</sup> Unfiltered aliquots were centrifuged for 10 minutes at 16,000g and particulate carbohydrates were extracted from pellets by KOH digestion and ethanol precipitation.<sup>22,24,25</sup> The 95% confidence interval on the calibration curve was smaller than 2 mg/L. During experiments, some noisy triplicates gave a standard deviation close to 5 mg/L.

As the substrate used for the experiments was glucose, the expected soluble microbial by-product (SMP) was acetate. Hence, the acetate concentration in filtered and diluted samples was measured by ion chromatography. However, the acetate concentration in diluted samples was always low and the data were noisy. Hence, SMP was estimated by subtracting the concentration of glucose COD from the soluble COD concentration.<sup>26,27</sup>

Protozoan and metazoan populations were quantified by individual count under a dark field microscope at 100× magnification.<sup>28</sup> Each count was performed in triplicate as well. The mean count was close to  $1\text{E} + 06$  org./L, hence 10 times lower than the values reported for the activated sludge process.<sup>29</sup> Sixty six percent of the population consisted of saccodine, and 30% of the observed microfauna were fixed ciliates. The inhibition method did not work well and seemed to simply shift the population of free ciliates and rotifers to a less evident type as saccodine. Predation and internal decay of active cells were then not distinguishable. Thus, it was assumed that the decay of the bacterial population included internal and external decay.<sup>30</sup>

During each batch experiment, the oxygen uptake rate (OUR) evaluation was performed with a LLS-type respirometer<sup>31</sup> according to Spérandio.<sup>32</sup> Mixed liquor was recycled from the batch reactor to the 250-mL closed respirometer with a peristaltic pump. Every 3 minutes and 30 seconds, the pump was running during 1 minute to renew at least three times the volume in the respirometer. The oxygen concentration was recorded every 2 seconds after a 30-seconds period of stabilization. After the pump stopped, the OUR was calculated of the slope of the regression curve of the dissolved oxygen (DO) data collected in the respiration chamber. The oxygen probe used was a WTW Cellox 325 and was connected to a data acquisition system.

For assessment of yields, the oxygen uptake rate evaluation was performed with a flowing gas-static liquid (LFS) respirometer.<sup>31</sup> The oxygen concentration was recorded every second. A first order filter was used to reduce noise in the signal.<sup>33</sup> The mass balance was performed by time integration of the data.

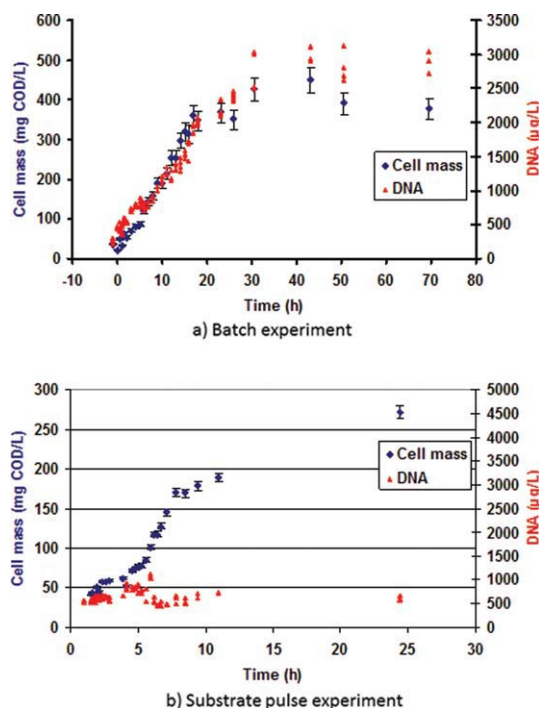


Figure 1. DNA and cell mass accumulation during the experiments.

(a) Batch experiment; (b) substrate pulse experiment.

## Experimental Results

Figure 1 shows the increase of cell mass and DNA in the experiments. The cell mass was assessed by subtracting inert material and glycogen from the particulate COD. In the batch experiment (Figure 1a), the cell mass and the DNA increased together. However, in the substrate pulse experiment (Figure 1b), an increase of cell mass is observed, but no significant increase in DNA.

Figure 2 presents the amount of nitrogen used for the production of cell constituents compared to the DNA increase. In the batch experiment (Figure 2a.), the slope of the regression line gives a specific nitrogen to cell DNA ratio ( $0.010 \text{ mgN}/\mu\text{g DNA}$ ).

No correlation was observed between nitrogen utilization and the DNA in the substrate pulse experiment (Figure 2b). However, nitrogen utilization was well correlated with the increase of cell mass (Figure 3). It is hypothesized that carbon and nitrogen are used for amino acid or proteins synthesis (here called precursors), which accumulate in the cells.

As shown in Figure 4, the observed cell mass (COD)/DNA ratio increased from 0.09 to  $0.22 \text{ mg COD}/\mu\text{g DNA}$  in the batch experiment. After the exhaustion of substrate, this ratio decreased again to  $0.14 \pm 0.03 \text{ mg COD}/\mu\text{g DNA}$  and keeps decreasing slowly for the following 50 hours. Hence, it is hypothesized that the specific COD of cells was the minimal observed value of  $0.09 \text{ mg COD}/\mu\text{g DNA}$ . Accordingly, the value of the COD/DNA ratio exceeding the basic value of  $0.09 \text{ mg COD}/\mu\text{g DNA}$  is assumed to be the COD of the precursors. The relative error on precursor assessment was lower than 25% for each triplicate, with a mean value of 15% for each data set for both experiments.

The ratio of nitrogen ( $0.010 \text{ mgN}/\mu\text{g DNA}$ ) and COD ( $0.14 \text{ mg COD}/\mu\text{g DNA}$ ) used per  $\mu\text{g}$  of DNA at the

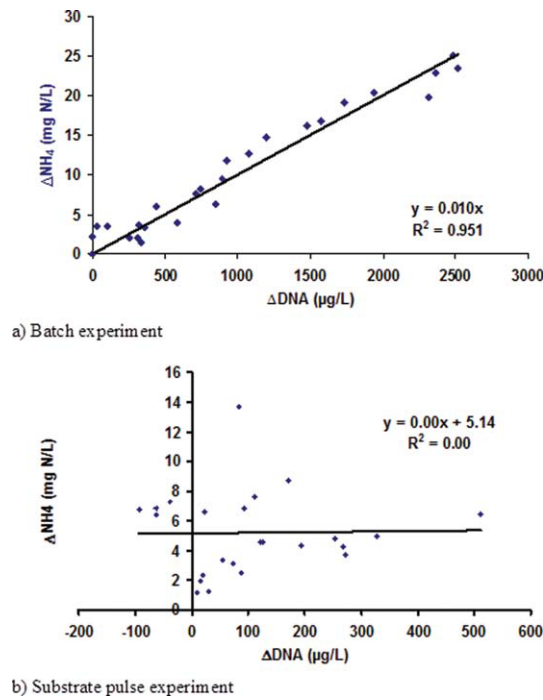


Figure 2. Nitrogen used and increase in DNA concentration. (a) Batch experiment; (b) substrate pulse experiment.

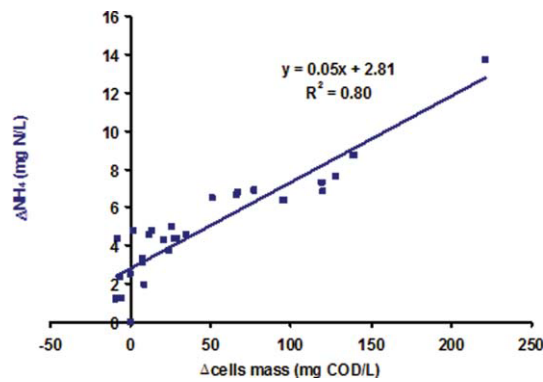


Figure 3. Increase of cell mass and nitrogen use in substrate pulse experiment.

substrate exhaustion points in the batch experiment gives the nitrogen fraction of the cells. The observed ratio ( $i_{NX}$ ) was 0.07 mg N/mg COD. This value is consistent with the default value of the biomass nitrogen content,  $i_{NBM} = 0.07$ , used in ASM3.<sup>34</sup>

The COD of the population  $X_H$  was then assessed using the DNA concentration and a conversion factor of 0.09 mg COD/ $\mu$ g DNA. This ratio seems high compared to a theoretical value of 0.03 mg COD/ $\mu$ g DNA based on 3% of DNA per cell mass.<sup>35</sup> However, considering the efficiency of the extraction protocol, the conversion factor is in agreement with the theoretical percentage of DNA in cells.

Figure 5a shows that at the start of the batch experiment, the oxygen uptake rate was high and unexpectedly, decreased sharply after a few minutes. Then, the oxygen uptake rate increased again until exhaustion of the substrate and dropped again as expected.

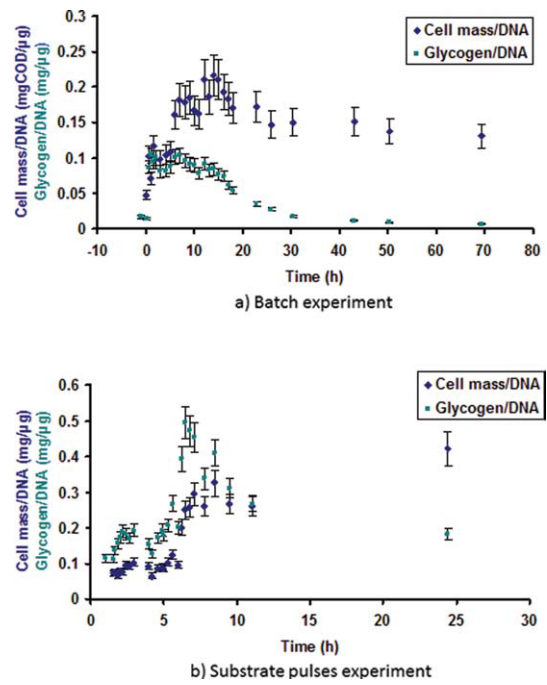


Figure 4. Variation of the cell mass/DNA ratio and glycogen/DNA ratio. (a) Batch experiment; (b) substrate pulses experiment.

In a first try, the growth rate was assessed using the evolution of the oxygen uptake rate and the DNA concentration during the exponential growth phase. The growth rate was assessed on time intervals of 3 hours, and it increased four-fold during the exponential phase. The analysis of OUR residuals stressed that the exponential relationship did not fit the data well (Figure 6a). The variance analysis ( $\alpha = 0.05$ ) showed that the error induced by the lack of fit was high and stressed that another model would provide a better fit.

Keener<sup>36</sup> have shown that the RNA level is positively correlated with the growth rate. They state that since the ribosome production is an autocatalytic reaction, in an unrestricted growing culture, the rate of ribosome accumulation (and rRNA), i.e., the increase of the growth rate, will increase with the square of the growth rate. Since the growth of a bacterial population is an autocatalytic reaction as is the rate of ribosome accumulation, then the RNA level theory predicts that after the removal of the carbon limitation on a slow growing culture, the increase of the population will follow a double exponential growth curve, as shown in Figure 4b. The residuals of this model fit are shown on Figure 6b.

In Figure 7, one can see that, after a first drop, the specific oxygen uptake rate (OUR/DNA) decreased slightly throughout the exponential growth phase. This observation is not in agreement with results found in literature<sup>37</sup> or to the RNA level theory. It raises questions about the need to model the RNA level for slow-growing biomass. With this in mind, the growth rate obtained from the OUR and from the DNA data were compared. The ratio of the equations of the two regression curves on Figure 5 gives a parabolic curve with a minimum near the 12th hour. Thus it was assumed that the downregulation of the OUR observed in the first hour of the experiment was extending and decreasing for several hours. It was concluded that until the 12th hour, the increase of the

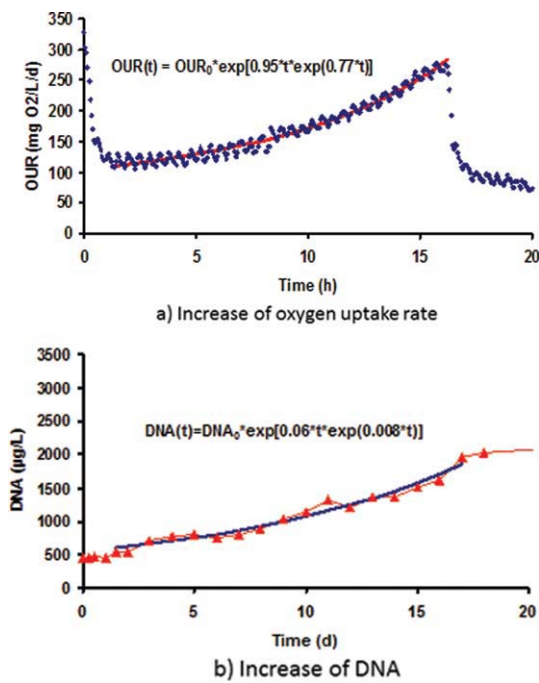


Figure 5. Growth rate assessment for the batch experiment.

(a) Increase of oxygen uptake rate; (b) increase of DNA.

specific OUR caused by the increase of the growth rate was masked by the downregulation of the substrate uptake rate observed in the first few hours.

The sharp decrease of OUR at the beginning of the experiment was a reproducible transient behavior. The peak in oxygen uptake rate corresponds to the high rate of substrate uptake and glycogen formation. In the first hour of the experiment, Figure 7 shows that the glycogen/DNA ratio in cells increased sharply while the OUR/DNA ratio decreased quickly, and then remained constant until exhaustion of the substrate. The accumulation capacity of the cells was evaluated by time integration of the OUR curve during the first hour.<sup>7</sup> Using this method, the initial accumulation capacity was estimated to be 0.09 mgCOD/ $\mu$ g DNA. This value fits the sharp increase of glycogen at the start of the experiment. It was concluded that the cells stored substrate as glycogen until the storage capacity was fully used and then the substrate uptake rate seems governed by the anabolic rate. Hence, the OUR drop observed at the beginning of the experiment seems correlated with the drop of the substrate uptake rate.

In Figure 4, one can observe that the cell mass COD/DNA increased after having completed the glycogen accumulation capacity. The increase of cell mass COD/DNA indicates a saturation of the anabolic fluxes. This observation is in agreement with the previous observation that the substrate uptake rate is first governed by the storage rate and afterward by the anabolism rate.

The increase of cell mass COD/DNA, called here the precursor accumulation, supports the assumption that the RNA level limits the growth rate when cells are suddenly exposed to high substrate concentrations. On the other hand, the nitrogen incorporation did not seem to be limiting for cell growth as precursors were accumulated after the storage capacity had been filled completely. However, the rate of

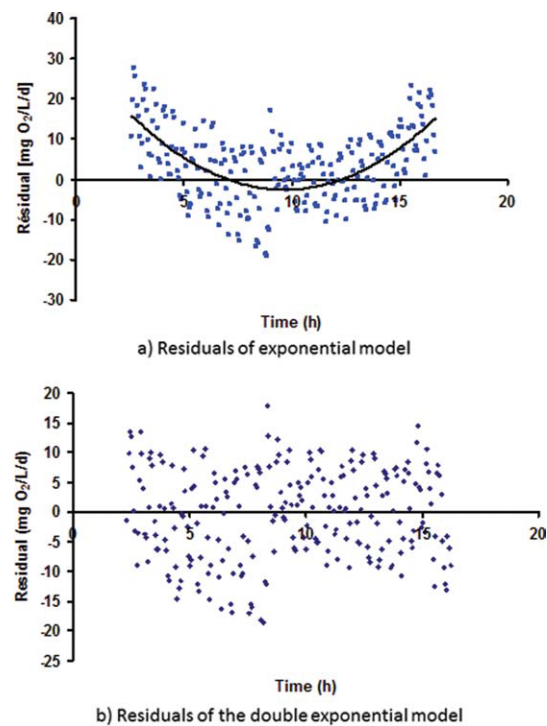


Figure 6. Residuals distribution of the growth models.

(a) Residuals of the exponential model; (b) residuals of the double exponential model.

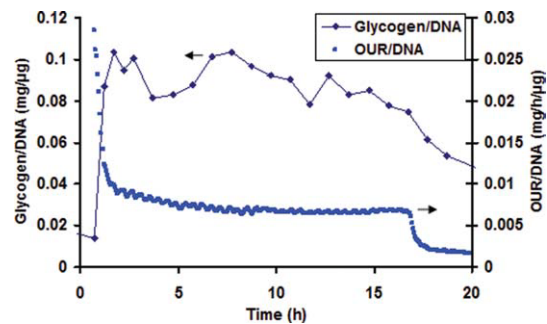


Figure 7. Fluctuations of the specific oxygen uptake rate and glycogen accumulation in the batch experiment.

precursor accumulation was lower than the maximal carbon uptake rate. Hence, in these conditions the carbon fluxes should not be the bottleneck of the growth process. We assumed that the imbalance of metabolic fluxes increased the energy charge (the adenylate charge ratio) and according to Preiss,<sup>38</sup> this induced the genetic expression of enzymes responsible for glycogen accumulation. Consequently, according to Chang<sup>8</sup> and Harper,<sup>39</sup> it was assumed that storage would be induced by an imbalance between the rates of assimilation of carbon and nitrogen. Therefore, for the purpose of modeling, accumulation of intracellular substrate caused by the imbalance in the uptake of carbon and nitrogen was used to describe the observed transient behaviors.

The resulting specific rates ( $r$ /DNA) and cell's composition ( $C$ /DNA) provide an assessment of the metabolic status of the bacterial population. This information should be used to assess the intrinsic values of parameters<sup>5</sup> in model development and calibration.

### The Proposed Model

Figure 8 shows the simplified model of carbon and nitrogen metabolism adopted here. In this figure, the capital letter S stands for soluble components, capital B stands for intracellular material, and X for particulate material. The soluble substrate is modeled by the  $S_S$  component, the utilization associated soluble microbial products by  $S_{MP}$ , and ammonia by  $S_{NH}$ . In the figure, intracellular substrates like G6P or pyruvate are modeled by  $B_S$ , while the amino acids and precursors are modeled by the  $B_P$  component, and the cell structure by  $X_H$ . The units of all these components are in mg/L.

In Figure 8, the arrows stand for enzymatic reactions. One arrow could stand for a sequence of several enzymatic reactions. In the model, the notation E refers to an enzymatic structure, and its units are in mg/L. When the enzymatic component is expressed as a specific value, the notation is expressed as  $E/X_H$  and its units are in mg/mg.

In Figure 8, two substrate transporter systems, the phosphoenolpyruvate transferase system (PTS) and a non-PTS system are modeled. According to Chang,<sup>8</sup> the PTS has a high capacity and is expressed at high substrate concentrations. The PTS consumes phosphoenolpyruvate (PEP) and produces an excess of pyruvate, which in turn inhibits the PTS.<sup>40</sup> The excess of pyruvate is then transformed in utilization associated soluble microbial products that are excreted.<sup>9,41</sup> The non-PTS system is subject to catabolic

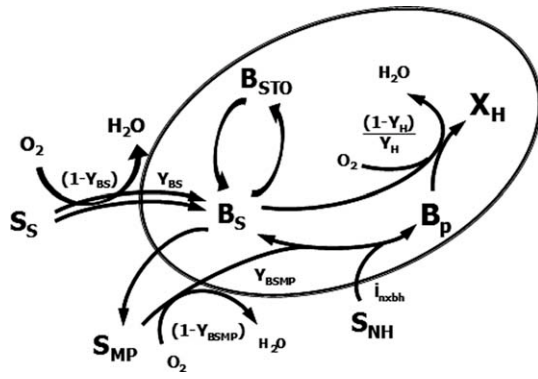


Figure 8. Schematic of metabolism.

repression and it is only present at lower growth rates.<sup>42</sup> Chen<sup>43</sup> showed also that the non-PTS has a lower capacity than the PTS, and Chang<sup>8</sup> observed that the non-PTS leads to a more balanced flux of carbon and nitrogen.

Aminoacid synthesis uses glutamate and metabolites of the tricarboxylic acid cycle.<sup>10</sup> Hence, nitrogen assimilation and glutamate availability positively regulate incorporation of carbon in the tricarboxylic acid cycle. Hence, in the model the  $B_P$  and the  $B_S$  components are used in saturation functions to mimic the regulation of the carbon uptake by the intracellular nitrogen availability or the excess of carbon and the saturation of the flux.

After exhaustion of the soluble substrate  $S_S$ , the excreted  $S_{MP}$  are taken up again but at a different branch point of the metabolism than  $S_S$ . They are then transformed in  $B_P$ .

A complete mathematical description of the model is given under Gujer matrix form in Tables 1–4. The arrows of Figure 8 are translated in their mathematical formulation.

To validate of the proposed metabolic model, simple model versions were tested on the experimental data presented in this paper. The best fit of the simple model versions did not fit at all at least one component or gave large deviation on several and were out of synchronism with rise and fall of some components like OUR and glycogen. Only the model versions which include the intracellular precursor component shown in Figure 8 allowed describing the down-regulation of substrate uptake and nitrogen incorporation into the cells. The proposed model is the simplest one tested that can describe all components and rates shown in the two comprehensive experimental datasets. The COD and nitrogen mass balance is modeled with 19 processes and 14 components (five of which are virtual enzymes) and the rate fluctuations are modeled with the increase and decay of the virtual enzymes. In comparison, the ASM3 model uses five processes and eight components to model the COD and nitrogen mass balance of heterotrophic biomass in aerobic conditions, but no modulation of the kinetic rate expressions is possible. Hence, the proposed model mainly introduces the modulation of the rates at the substrate uptake enzyme levels and at the rRNA synthesis level.

In Table 1, several process rates are modulated by the enzymes concentration (E) and are regulated by the concentration of the enzymes' substrates. The ratio  $B_{PSS}/X_H$  in

Table 1. Processes Description

Rate	Process rate description	Process rate equation:
r1	Increase of $B_S$ (high affinity system)	$k_{Bsha}^{max} * E_{Bsha} * M_{Ssha} * M_{So}$
r2	Increase of $B_S$ (low affinity system)	$k_{Bsla}^{max} * E_{Bsla} * M_{Ssla} * I_{bs}^{max}$
r3	Increase of $B_{STO}$	$k_{sto}^{max} * E_{STO} * M_{Bsto} * M_B^{max}$
r4	Uptake of $S_{MP}$	$k_{BSMP}^{max} * E_{BS(SMP)} * M_{SMP} * I_{ssha}$
r5	Increase of $B_P$	$k_{Bp}^{max} * M_{NH} * M_{Bs} * X_H$
r6	Aerobic growth of heterotrophs and $E_G$	$\mu_{Hmax}^{int} / f_{PSS}^{max} * B_{PSS} / X_H * M_{So} * M_{Bs} * M_{Bp} * X_H$
r7	Aerobic growth of $B_{PSS}$	$k_{PSS} * B_{PSS} * M_{So} * M_{Bs} * M_{Bp}$
r8	Increase of $E_{STO}$	$\alpha_{E_{sto}} * B_{PSS} * M_{Bsof} * M_{So} * M_{Bs} * M_{Bp}$
r9	Increase of $E_{Bsha}$	$\alpha_{E_{Bsha}} * B_{PSS} * M_{Ssha} * M_{So} * M_{Bs} * M_{Bp} * I_{Ssla}$
r10	Increase of $E_{Bsla}$	$\alpha_{E_{Bsla}} * B_{PSS} * M_{Ssla} * M_{So} * M_{Bs} * M_{Bp}$
r11	Increase of $E_{Bs(SMP)}$	$\alpha_{E_{BSMP}} * B_{PSS} * M_{SMP} * I_{Ssha} * M_{So} * M_{Bs} * M_{Bp}$
r12	Release of $S_{MP}$	$k_{Bs}^{max} * M_{Bsof} * B_S$
r13	Degradation of $B_{STO}$	$\delta k_{sto}^{max} * E_{STO} * M_{STO} * I_{Ssla}$
r14	Decay of $B_P$	$b_{Bp} * B_P$
r15	Decay of $B_{PSS}$	$b_{PSS} * B_{PSS}$
r16	Decay of $E_{STO}$	$\beta_{E_{sto}} * E_{STO}$
r17	Decay of $E_{Bsha}$	$\beta_{E_{Bsha}} * E_{Bsha}$
r18	Decay of $E_{Bsla}$	$\beta_{E_{Bsla}} * E_{Bsla}$
r19	Decay of $E_{Bs(SMP)}$	$\beta_{E_{BSMP}} * E_{Bs(SMP)}$
r20	Decay of $X_H$	$b_H * I_{ssla} * X_H$

process 6 (r6) reflects the metabolic state of the active biomass. It will change the  $\mu_H$  value according to the ribosome level in the cells following the RNA limiting theory. Since the synthesis of ribosomes is an autocatalytic process, the increase of the  $B_{PSS}$  component is modeled by using the  $B_{PSS}$  component and its intrinsic increase rate  $k_{PSS}$  in r7 (Table 3). The dependency on the availability of amino acids is mimicked by including the  $B_P$  intracellular precursors term.

The messenger RNA (mRNA) is not considered in this model. As it has a half-life close to 2 minutes, it quickly reaches a quasi-steady-state concentration.<sup>44</sup>

In the model, the variable  $B_P$  has COD units. Hence, the active biomass COD is now composed of an amount of structural component ( $X_H$ ) and a variable fraction, the "bio-synthetic constituent" ( $B_P$ ). The constituent  $B_P$  is intracellular, and the mathematical description of biomass then becomes ( $X_H + B_P + B_S$ ). This description agrees with the description of biomass proposed by Masson<sup>45</sup> and van den Berg.<sup>46</sup> Thus, in the model, the specific value of the biomass COD ( $(X_H + B_P + B_S)/X_H$ ) will rise and fall with  $B_P$ . Accordingly, in this paper, the storage capacity is the maximal  $B_{STO}/X_H$  ratio, and the accumulation capacity is the maximal  $(B_{STO} + B_P + B_S)/X_H$  ratio.

The decay of  $B_P$  ( $\beta_{BP}$ ) is a continuous process and will thus occur both during growth and starvation. During starva-

tion, the active biomass ( $X_H$ ) will use  $B_P$  to produce the energy required for growth on this component. The  $B_P$  component is then transformed in  $B_S$  and  $S$ . The cycling of this component will use a part of the COD for respiration. This will be assumed to be the maintenance process. It will increase with the size of  $B_P$ .

In the literature it is recognized that cell death of most prokaryotes can be induced by the action of a toxin-antitoxin couple (TA).<sup>47-50</sup> The TA is produced by cells during growth, and the antitoxin counteracts the toxin effect. Only a short time after substrate depletion, the antitoxin is depleted and the toxin can turn on its bactericidal effect. In the proposed model the decay rate of active cells (r19) depends on the availability of substrate. Thus, the decay rate would be regulated inversely to the growth rate.<sup>51</sup> The decay process leads mainly to endogenous respiration.

The production of the enzymes is modeled by including a dependency on  $B_{PSS}$  and  $B_P$  components. The decay of  $B_{PSS}$  and enzyme components (processes r14 to r18) are endogenous processes described as first order reactions

**Table 2. Description of Saturation and Inhibition Functions**

Description of Saturation and Inhibition Functions	
$M_{Bs}$	$(B_S/X_H)/(K_{Bs} + (B_S/X_H))$
$M_{Bp}$	$B_P/X_H/(K_{Bp} + B_P/X_H)$
$M_{SMP}$	$S_{MP}/(K_{SMP} + S_{MP})$
$M_{Ssha}$	$S_S/(S_S + K_{Ssha})$
$M_{Ssla}$	$S_S/(S_S + K_{Ssla})$
$M_{NH}$	$S_{NH}/(K_{NH} + S_{NH})$
$M_{So}$	$S_O/(S_O + K_O)$
$M_{Bsto}$	$(B_{STO}/X_H)*(B_S/X_H)$
$M_{STO}$	$(B_{STO}/X_H)/(K_{STO} + B_{STO}/X_H)$
$I_{bs}$	$(K_{ibs}/(K_{ibs} + B_S/X_H))$
$I_{Ssha}$	$K_{Ssha}/(K_{Ssha} + S_S)$
$I_{Ssla}$	$(K_{Ssla}/(S_S + K_{Ssla}))$
$M_{Bsof}$	$(B_S/X_H)/(K_{bsof} + (B_S/X_H))$
$M_B^{max}$	$(f_{STO}^{max} - B_{STO}/X_H)/(K_{isto} + f_{STO}^{max} - B_{STO}/X_H)$

**Table 3. Stoichiometry of Enzymatic Components**

Rate, Units	$B_{PSS}$ , g/g	$E_{STO}$ , g/g	$E_{BSha}$ , g/g	$E_{BSla}$ , g/g	$E_{BS(SMP)}$ , g/g
r1					
r2					
r3					
r4					
r5					
r6					
r7	1				
r8		1			
r9			1		
r10				1	
r11					1
r12					
r13					
r14					
r15	-1				
r16		-1			
r17			-1		
r18				-1	
r19					-1
r20	$-B_{PSS}/X_H$	$-E_{STO}/X_H$	$-E_{BSha}/X_H$	$-E_{BSla}/X_H$	$-E_{BS(SMP)}/X_H$

**Table 4. Stoichiometry of Intracellular, Soluble and Particulated Components**

Rate, Units	$S_O$ , gCOD/m <sup>3</sup>	$S_S$ , gCOD/m <sup>3</sup>	$B_S$ , gCOD/m <sup>3</sup>	$B_{STO}$ , gCOD/m <sup>3</sup>	$S_{NH}$ , gN/m <sup>3</sup>	$B_P$ , gCOD/m <sup>3</sup>	$X_H$ , gCOD/m <sup>3</sup>	$S_{MP}$ , gCOD/m <sup>3</sup>	$X_{ii}$ , gCOD/m <sup>3</sup>
r1	$-(1 - Y_{BS})$	-1	$Y_{BS}$						
r2	$-(1 - Y_{BS})$	-1	$Y_{BS}$						
r3			-1	1					
r4	$-(1 - Y_{SMP})$				$-i_{nx} * Y_{SMP}$	$Y_{SMP}$		-1	
r5			-1		$-i_{nx}$	1			
r6	$-(1 - Y_H)/Y_H$		$-(1 - Y_H)/Y_H$			-1	1		
r7									
r8									
r9									
r10									
r11									
r12			-1					1	
r13			1	-1					
r14			1		$i_{nx}$	-1			
r15									
r16									
r17									
r18									
r19									
r20	$-(1 - fu) * (1 + B_S/X_H + B_{STO}/X_H + B_P/X_H)$		$-B_S/X_H$	$-B_{STO}/X_H$	$(1 - fu) * i_{nx} * (1 + B_P/X_H)$	$-B_P/X_H$	-1		$fu * (1 + B_S/X_H + B_{STO}/X_H + B_P/X_H)$

characterized by the “endogenous” rate constants  $b$ . This formulation is similar to the one used by Baloo<sup>52</sup> for the decay of enzymes.

Modeling of storage (process r3) is done through a single reaction for glycogen<sup>12</sup> and for PHB.<sup>53</sup> As proposed by Dircks et al.<sup>12</sup> and Beun et al.,<sup>53</sup> a maximal fraction ( $f_{STO}^{max}$ ) of  $B_{STO}$  in the cell is included in the regulation of the process. This fraction parameter is also included in the saturation function as proposed in ASM2<sup>34</sup> for polyphosphate.

Soluble microbial product ( $S_{MP}$ ) formation was significant during the experiments performed, and the COD mass balance would take it into account. In process r12, the constant  $k_{r_{Bs}}^{max}$  therefore mimics the outward diffusion of metabolites through the cell membrane.

### Assessment of Yields and Fractions

A number of new parameters are proposed in the model. Hence, new methods were required for parameter identification of yields and fractions.

The COD of the population  $X_H$  was assessed using the DNA concentration and a conversion factor of 0.09 mg COD/ $\mu$ g DNA. This ratio seems high compared to a theoretical value of 0.03 mg COD/ $\mu$ g DNA based on 3% of DNA per cell mass.<sup>35</sup> Considering the efficiency of the extraction protocol, the conversion factor is in agreement with the theoretical percentage of DNA in cells.

The ratio of nitrogen (0.010 mgN/ $\mu$ g DNA) and COD (0.14 mg COD/ $\mu$ g DNA) used per  $\mu$ g of DNA at the substrate exhaustion in the batch experiment gives the nitrogen fraction into cells. The observed ratio ( $i_{NX}$ ) was 0.07 mg N/mg COD. This value is consistent with the default value of the biomass nitrogen content,  $i_{NBM} = 0.07$ , used in ASM3.<sup>34</sup>

The yields were estimated in three steps. In the first step, the yield of intracellular substrate on exogenous substrate ( $Y_{Bs}$ ) has been calculated from a COD mass balance during a substrate pulse in a respirometric experiment.<sup>54</sup> The oxygen consumption was assumed as negative COD.

As discussed by Vanrolleghem,<sup>54</sup> in this short pulse experiment all glucose was stored as glycogen. The following equation was applied to assess the yield of intracellular substrate on exogenous substrate  $Y_{Bs}$ :

$$Y_{Bs} = 1 - \frac{\int r_{O_2}(t)dt}{\Delta COD_{consumed}} \quad (1)$$

The experiment was repeated three times, and the  $Y_{Bs}$  mean value was close to 0.9 g COD/g COD.

Then, in the second step, the yield of cell constituents on intracellular substrate ( $Y_{H/Bs}$ ) has been estimated from a COD mass balance on the batch experimental data over the exponential growth phase. Regrowth and respiration on dead cells was not taken into account since the cell death can be assumed negligible under the exponential growth phase, as discussed before. The equation proposed<sup>54</sup> to model the respiration on readily biodegradable substrate was modified to take into account the respiration associated to substrate that is taken up and is accumulated as intracellular materials. The following equation was applied to evaluate  $Y_H$ :

$$Y_{XH} = \frac{\left[ \frac{1 - \int r_{O_2}(t)dt - (\Delta B_{STO} + \Delta B_P) * (1 - Y_{Bs}) / Y_{Bs}}{\Delta COD_{consumed} - \Delta B_{STO} - \Delta B_P} \right]}{Y_{Bs}} \quad (2)$$

The overall yield of  $X_H$  on exogenous substrate was  $Y_{Bs} * Y_H = 0.6$  g COD/g COD. Thus, the  $Y_H$  found on data of the batch experiment was 0.67 g COD/g COD. For a biomass growing on glucose, Dircks<sup>12</sup> observed similar values.

Finally, in the third step the yield of intracellular precursors on  $S_{MP}$  ( $Y_{SMP}$ ) was chosen according to the  $Y_{STO}$  default value in ASM3.<sup>34</sup> The yield of  $B_P$  on  $S_{MP}$  was set to 0.8 g COD/g COD. The value for the uptake rate of  $S_{MP}$  was then chosen to fit the model output on the  $S_{MP}$ ,  $B_P$  and OUR data.

### Fitting the Model to Data

The model was implemented in GPS-X© using the Model Developer of Hydromantis Inc. Figures 8–11 show the fit of the model to the data. The proposed model is a simplified view of complex biochemical pathways of microorganisms. The process rate equations do not aim to model specific enzymes, but whole pathways. Hence, values of kinetic constants found in biochemistry literature were not useful for the fitting of data. For some parameters, default values of ASM parameters were used as initial values; however, since new processes and new process descriptions were introduced in the model, different parameters values were required to fit the data.

The value of each constant was determined using different components or ratio, different periods in the various experiments performed, thus allowing some independency in identification process of constant values. Descriptions of insensitive process rate or those going critical were modified during this procedure giving the proposed version of the model. Then, a sequential optimization of constants performed several times in a looping process was used as

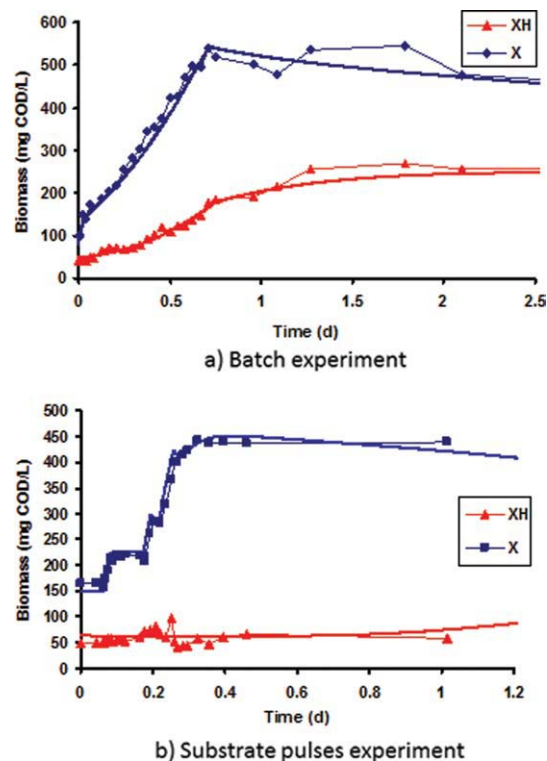


Figure 9. Increase of active biomass (XH) and total biomass (X) during the experiments.

(a) Batch experiment; (b) substrate pulses experiment.

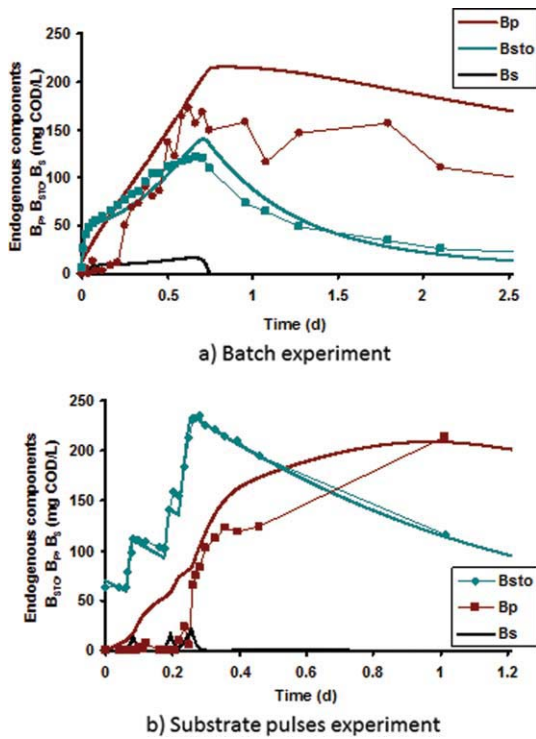


Figure 10. Evolution of intracellular components. (a) Batch experiment; (b) substrate pulses experiment.

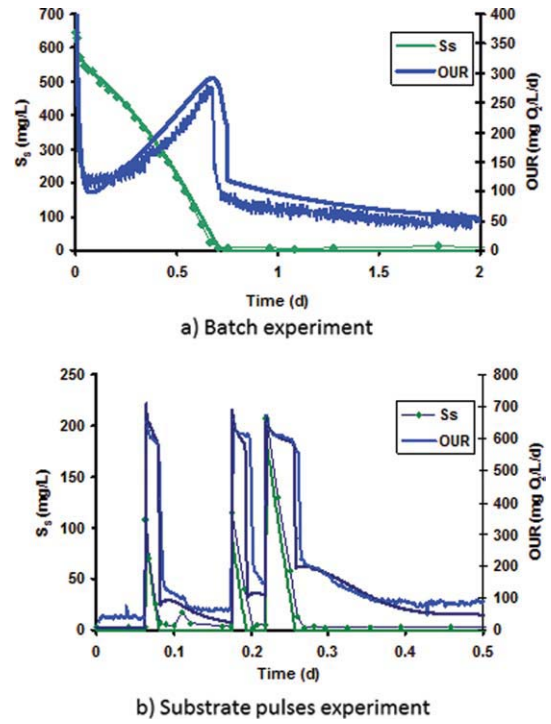


Figure 11. Evolution of soluble substrate and OUR. (a) Batch experiment; (b) substrate pulses experiment.

calibration procedure. The looping process of the sequential optimization shows some dependency in the constants values. Monte-Carlo simulations and systematic sensitivity analysis of the model remain to be performed.

For the batch experiment, the mean deviation between the model response and the data is lower than 6% of the COD for the total biomass ( $X$ ) and also for the COD of the soluble substrate ( $S_S$ ). The total biomass is the sum of the active biomass ( $X_H$ ), the intracellular materials ( $B_S$ ,  $B_{STO}$ ,  $B_P$ ), and the inert material ( $X_{ii}$ ). The mean difference between the model predictions and the data was lower than 9% for the active biomass ( $X_H$ ), lower than 12% for glycogen ( $B_{STO}$ ) and substrate ( $S_S$ ), lower than 15% for the OUR, and lower than 6% for the nitrogen component ( $S_{NH}$ ). Obviously, the deviation between the model response and the data becomes large when the data decreases to low values.

The mean deviations observed between the model output and the data in the substrate pulse experiment were of the same magnitude, albeit larger for the OUR and the active biomass ( $X_H$ ). The larger deviation of the OUR was ascribed to the lack of synchronization between the model output and the data at the sharp increase or drop off of the OUR. The deviation on the active biomass was blamed to the variation of the data since no growth of  $X_H$  was observed during this experiment.

As can be seen on Figures 10 and 12, the deviation between the model response ( $B_P$  and  $S_{MP}$ ) and the endogenous precursor and soluble microbial product data is large. These two components were not assessed directly with experimental measurements but after some manipulation of the COD data. Still, the model outputs represented the trends observed in the data.

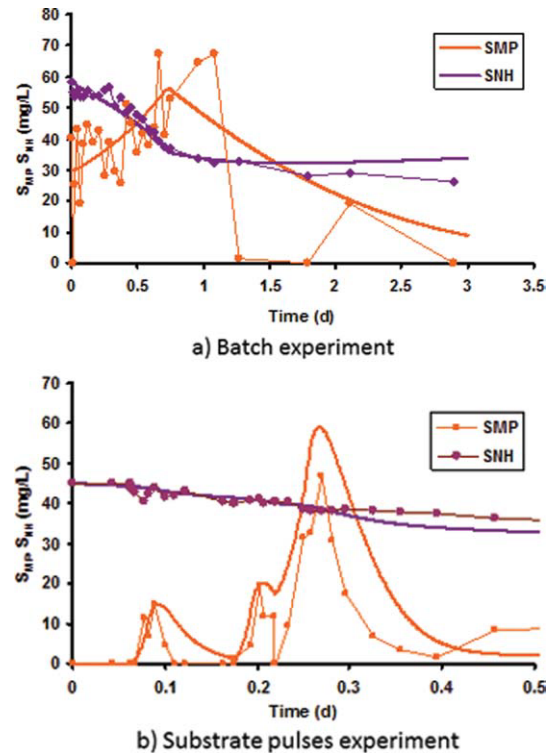


Figure 12. Evolution of soluble microbial products and ammonia. (a) Batch experiment; (b) substrate pulses experiment.

## Discussion

The proposed model is based on biochemical concepts. Thus, the main objective of the modeling exercise was to perform a validation of the experimental methods and the proposed model make-up. For modeling of pure cultures, Narang and coworkers<sup>44,55</sup> used dry weight as basic unit to assess cell density. This is not possible in wastewater treatment since various kinds of particulate materials are coming with the influent and materials arising from decay of cells are accumulated in the system. In this paper, DNA was used as a basic unit to assess active biomass ( $X_H$ ). Exogenous DNA, resulting of decay of biomass was removed from suspended solids using crown ether. The intracellular DNA was then extracted and converted in COD using a stoichiometric coefficient. Note that another extraction protocol of DNA will probably give a different efficiency of extraction and thus a different stoichiometric coefficient.

Figure 9 shows that the used yields allow to adequately predict the active biomass ( $X_H$ ) and total biomass ( $X$ ) evolution. The stoichiometric coefficient of 0.09 mg COD/ $\mu$ g DNA seems to give a consistent evaluation of the active population of cells all along the experiments, even though the population increased fivefold.

On the other hand, no increase of the population was observed during the substrate pulse experiment as confirmed by the DNA data and the maximal oxygen uptake rate. Still, the substrate added to the mixed liquor in the substrate pulse and the batch experiments was 430 mg COD/L (doses of 108, 115, and 207 mg/L) and 630 mg COD/L, respectively, for an initial concentration of biomass of 50 and 63 mg COD/L, respectively. In the substrate pulse experiment, most of the substrate COD was accumulated in storage product and precursor materials, and a no growth period of 24 hours was observed. In the batch experiment, exponential growth occurred during the same period as COD was converted in active cell material.

It was not possible to fit the model on the data of these two experiments using a single set of parameters without modeling the RNA-level with the  $B_{PSS}$  component. Accordingly, sensitivity analysis showed that response of a simple model version is sensitive to the initial  $f_{PSS}$  value for various kinds of experiments.<sup>3</sup> This fraction allowed to model the no growth observed in the pulse experiment, and the growth rate increase in the batch experiment.

In Figure 11, it is evident that the inhibition of the OUR was quite larger in the batch experiment than in the substrate pulse experiment. The substrate uptake rates decrease along the same pattern. In the batch experiment, the initial OUR and substrate uptake rate are at least fourfold higher than the rates after the inhibition. In the substrate pulse experiment, the initial OUR and substrate uptake rate are only 15% higher than the rates after the inhibition.

In the simulation of the batch experiment, the PTS (r2 in Table 1) was highly expressed and the non-PTS (r1 in Table 1) was expressed at a low level. After the PTS was inhibited, the transport rate was low and balanced with the growth rate of cells. In the simulation of the substrate pulse experiment, the non-PTS (r1) was highly expressed and the PTS (r2) was expressed at a lower level. After the PTS was inhibited, the non-PTS transport rate was high and not in balance with the growth rate of the cells. Then  $B_P$  accumulated in the biomass of the substrate pulse experiment and remained at a low level in the sludge of the batch experiment, as also observed in the experimental data.

At the end of the substrate pulse experiment, the glycogen/DNA ratio was five times the maximal fraction observed in the batch experiment. Dircks<sup>12</sup> proposed a detailed metabolic model for glycogen accumulating organisms, but the authors set the glycogen fraction as a fixed value. In the experiments presented in this paper, short rest periods in between substrate pulses increased the maximal storage capacity of the biomass. This adaptation of cells was not taken into account in the model.<sup>12</sup> Thus, the maximal fraction ( $f_{STO}^{max}$ ) of storage material had to be adjusted to fit the two experiments. The mechanism regulating the maximal value of the glycogen fraction could not be elucidated in this study. Further research is required to understand how this biomass characteristic is regulated.

As discussed earlier, in addition to the  $B_{STO}$  component, the data of the substrate pulse experiment showed that a nitrogenous component was accumulating in the cells (Figure 10b). Moreover, in Figure 12b, the data of this experiment reveal a production of  $S_{MP}$  when  $B_P$  increased. This is confirmed by the finding that accumulation of intracellular metabolites favors release of  $S_{MP}$ .<sup>56</sup>

In our opinion, the filling of the glycogen storage capacity followed by the accumulation of the nitrogenous component, and afterward by the release of soluble microbial products, indicates a sequence in saturation of the anabolic flux.

The saturation of the flux is modeled using the  $B_P/X_H$  ratio. In the model, the production rate of  $B_P$  can be higher than the growth rate and lower than the substrate uptake rate. In such conditions, when substrate is taken up, the  $B_P/X_H$  and the  $B_S/X_H$  ratio increase. The  $B_S/X_H$  ratio is used in saturation functions for regulation of the  $S_S$  uptake processes and this in turn affects the saturation of the anabolic flux.

However, from the various conditions applied in these two experiments, it could be concluded that the  $S_{MP}$  production was not proportional to the substrate taken up or to the biomass concentration, and moreover it was not correlated to the growth rate. Therefore, it appears that the regulation dynamics of this process is complex and a Luedeking–Piret type relationship<sup>57</sup> or an exponential relationship of the growth rate<sup>26</sup> were found insufficient to describe all the observed dynamics of the  $S_{MP}$  production.

In the proposed model, the rate of  $S_{MP}$  production was assumed to be a diffusion process through the cell membrane proportional to the  $B_S$  concentration. However, the diffusion coefficient had to be changed to fit the batch and the substrate pulse experiment. Simulation of the varying  $S_{MP}$  production could be improved by modeling an enzyme-catalyzed process.<sup>58</sup> The initial concentration of this enzyme would then be adjusted to fit the rate of the process on each experiment, but more information is needed on the regulation mechanisms of this process.

After short starvation periods, all substrate of a pulse was found to be taken up by the biomass. After a short peak, the OUR decreased and remained constant until the exhaustion of the substrate (Figure 11). The storage product ( $B_{STO}$ ) increased steadily until exhaustion of the substrate (Figure 10b). Unlike what was observed in the batch experiment, the initial peak of OUR cannot be associated to the regulation of the storage process rate. Therefore, in the substrate pulse experiment, in addition to the storage process, another mechanism must be regulating the substrate uptake. The short peaks of OUR observed after each substrate pulse were thus associated with saturation of the metabolic flux. This

hypothesis is supported by the discussion on the unbalanced uptake of carbon and nitrogen and is confirmed by the accumulation of the precursor component  $B_P$  and by the observed production of  $S_{MP}$ .

The tailing of the OUR after the substrate pulses was correlated to the re-uptake of soluble microbial products ( $S_{MP}$ ). Indeed, the decrease of the storage materials  $B_{STO}$  and  $B_P$  was not sufficient to explain the tailing of the OUR. On the other hand, simulations of the  $S_{MP}$  uptake gave good agreement with the data.

Additionally, even by using the data from the two experiments, it was not possible to extract information about the production of the enzymes. The objective of using enzyme concentrations in the model was to be able to take into account the history of the biomass. The counterpart of this is that simulations were sensitive to initial enzyme concentrations and that gave additional degrees of freedom to fit the data. Therefore, the model was run to fit data of a start-up experiment which ran over 25 days (data not shown). Using the parameter values given in Tables A2–A4, the model described the evolution of the COD all along the experiment. The simulations were not sensitive to the initial concentrations of enzymes but to the production rate ( $\alpha_E$ ) of the enzyme. This means that in the proposed model, simulations could be done according to the history of the biomass to determine the initial level of the enzymes for the starting point of a given experiment. It can be concluded that more information is needed to enhance the modeling of transients induced by process induction.

### Conclusion

The proposed experimental method seems to give a reliable evaluation of the model components and the model structure presents a consistent assessment of the process dynamics. The components/DNA and rate/DNA ratios could be used to assess the metabolic status of the biomass, and this rich information allows assessing levels of intracellular components which could not be assessed in another way.

The data demonstrated the accumulation of precursors ( $B_P$ ) when the biomass was exposed to large pulses of substrate. Since synthesis of precursor can be higher than their use, this supports the assumption that the RNA-level limits the growth rate when cells are exposed to high substrate concentrations.

Modeling the imbalance of the uptake rate of carbon and nitrogen gave good results in the simulation of the observed transient behaviors. The model parameters were calibrated on the observed data and the paper shows that the observed transient behaviors can be explained with the proposed metabolic network. Thus, the fit of the model on the experimental data supports the proposed regulation pattern and the tested hypothesis.

The model needs some improvements to properly model some phenomena observed during the experiments. Further studies are required to understand how the maximal fraction of storage material a cell can hold is regulated. Also, simulation of the  $S_{MP}$  production should be enhanced by modeling it as an enzyme catalyzed process, but more information is needed on the induction of the processes.

On the other hand, some simplifications to the model can be proposed if the simulations aim to describe the behavior

of the biomass when the storage capacity is not completely used. According to the sequence observed in fulfilment of the accumulation capacity and SMP production, saturation of the anabolic flux does not seem to be observable when the storage capacity is not completely used, and modeling of the component  $B_S$ ,  $B_P$  and  $S_{MP}$  is then not useful.

Further investigations using RNA-based techniques are required to support the proposed protocol and assumptions. These techniques could be used to validate the proposed component to model the rRNA level and the maximal growth rate fluctuations.<sup>3</sup> Also, more information is needed to enhance the modeling of transients induced by induction of processes like substrate uptake, soluble microbial product formation, and storage.

### Acknowledgments

The authors thank the NSERC (Canada) for financing this project). Peter Vanrolleghem holds the Canada Research Chair on Water Quality Modelling.

### Literature Cited

1. Saikaly PE, Stroot PG, Oerther DB. Use of 16S rRNA gene terminal restriction fragment analysis to assess the impact of solids retention time on the bacterial diversity of activated sludge. *Appl Environ Microbiol.* 2005;71:5814–5822.
2. Lavallée B, Frigon D, Lessard P, Vanrolleghem PA, Yuan Z, van Loosdrecht MCM. Modelling using rRNA-structured biomass models. *Wat Sci Technol.* 2009;59:661–671.
3. Hao X, Wang Q, Zhang X, Cao Y, van Loosdrecht MCM. Experimental evaluation of decrease in bacterial activity due to cell death and activity decay in activated sludge. *Wat Res.* 2009;43:3604–3612.
4. Grady CPL, Smets, BF, Barbeau, DS. Variability in kinetic parameter estimates: a review of possible causes and a proposed terminology. *Wat Res.* 1996;30:742–748.
5. Lavallée B, Lessard P, Vanrolleghem PA. Review of prokaryote metabolism in view of modeling microbial adaptation from fast growth to starvation conditions. *J Environ Eng Sci.* 2005;4:517–532.
6. Lavallée B, Lessard P, Vanrolleghem PA. Modeling the metabolic adaptations of the biomass under rapid growth and starvation conditions in the activated sludge process. *J Environ Eng Sci.* 2005;4:533–548.
7. Cech JS, Chudoba J. Influence of accumulation capacity of activated sludge microorganisms on kinetics of glucose removal. *Wat Res.* 1983;17:659–666.
8. Chang DE, Shin S, Rhee JS, Pan JG. Acetate metabolism in a mutant of *Escherichia coli* W3110: importance of maintaining acetyl coenzyme A flux for growth and survival. *J Bacteriol.* 1999;181:6656–6663.
9. Aon JC, Cortassa S. Involvement of nitrogen metabolism in the triggering of ethanol fermentation in aerobic chemostat cultures of *Saccharomyces cerevisiae*. *Metabolic Eng.* 2001;3:250–264.
10. Merrick MJ, Edwards RA. Nitrogen control in bacteria. *Microbiol Rev.* 1995;59:604–622.
11. Vishignac W, Santer M. The thiobacilli. *Bacteriol. Rev.* 1975;21:195–213.
12. Dircks K, Beun JJ, van Loosdrecht MCM, Heijnen JJ, Henze M. Glycogen metabolism in aerobic mixed cultures. *Biotechnol Bioeng.* 2001;73:85–94.
13. van Dongen LGJM, Jetten MSM, van Loosdrecht MCM. *The Combined Sharon/Anamox Process A Sustainable Method for N-removal from Sludge Water.* UK: IWA Publishing; 2001.
14. Maurines-Carboneill C, Pernelle JJ, Morin L, Sachon G, Leblon G. Relevance of the INT test response as an indicator of ETS activity in monitoring heterotrophic aerobic bacterial populations in activated sludge. *Wat Res.* 1998;32:1213–1221.

15. Schaechter M, Maaloe O, Kjeldgaard NO. Dependency on medium and temperature of cell size and chemical composition during balanced growth of *Salmonella typhimurium*. *J General Microbiol.* 1958;19:592–606.
16. Picard C, Ponsoonnet C, Paget E, Nesme X, and Simonet P. Detection and enumeration of bacteria in soil by direct DNA extraction and polymerase chain reaction. *Appl Environ Microbiol.* 1992;58:2717–2722.
17. Shen LL, Kohlbrenner WE, Weigl D, Baranowski J. Mechanism of quinolone inhibition of DNA gyrase, appearance of unique norfloxacin binding sites in enzyme-DNA complexes. *J Biol Chem.* 1989;264:2973–2978.
18. Wurtz S, Spaeth R, Hinderberger A, Griebe T, Flemming HC, Wilderer PA. A new method for extraction of extracellular polymeric substances from biofilms and activated sludge suitable for direct quantification of sorbed metals. *Wat Sci Technol.* 2001;43:25–31.
19. Yu Z and Mohn WW. Killing two birds with one stone: simultaneous extraction of DNA and RNA from activated sludge biomass. *Can J Microbiol.* 1999;45:269–272.
20. Paul JH, Myers B. Fluorometric determination of DNA in aquatic microorganisms by use of Hoechst 33258. *Appl Environ Microbiol.* 1982;43:1393–1399.
21. APHA, AWWA, WPCF. *Standard Methods for the Examination of Water and Wastewater*, American Public Health Association; 1998.
22. Daniels L, Hanson R, Phillips JA. Chemical analysis. In: Gerhardt P, Murray RGE, Wood WA, Krieg NR, editors. *Methods for General and Molecular Bacteriology*. Washington: American Society for Microbiology; 1994:512–554.
23. Herbert D, Phipps PJ, Strange RE. Chemical analysis of microbial cells. In: Norris JR, Ribbons DW, editors. *Methods in Microbiology*. London and New York: Academic Press; 1971:209–344.
24. Wang JC, Park JK, Whang LM. Comparison of fatty acid composition and kinetics of phosphorus-accumulating organisms and glycogen-accumulating organisms. *Wat Environ Res.* 2001;73:704–710.
25. Makinoshima H, Aizawa SI, Hayashi H, Miki T, Nishimura A, Ishihama A. Growth phase-couple alterations in cell structure and function of *Escherichia coli*. *J Bacteriol.* 2003;185:1338–1345.
26. Hao OJ, Lau AO. Kinetics of microbial by-product formation in chemostat pure cultures. *Environ Eng ASCE.* 1988;114:1097–1115.
27. Grady CLP, Harlow LJ, Riesing RR. Effects of growth rate and influent substrate concentration on effluent quality from chemostats containing bacteria in pure and mixed culture. *Biotechnol Bioeng.* 1972;14:391–410.
28. Védry B. *Les biomasses épuratrices*. Seine-Normandie: Agence de l'eau, 1996.
29. Ratsak CH, Maarsen KA, Kooijman SALM. Effect of protozoa on carbon mineralization in activated sludge. *Wat Res.* 1996;30:1–12.
30. van Loosdrecht MCM, Henze M. Maintenance, endogenous respiration, lysis, decay and predation. *Wat Sci Technol.* 1999;39:107–117.
31. Spanjers H, Vanrolleghem PA, Olson G, Dold PL. *Respirometry in control of the activated sludge process: Principles*. Scientific and technical report no. 7. IAWQ, 1998.
32. Spérandio M. *Développement d'une procédure de compartimentation d'une eau résiduaire urbaine et application à la modélisation dynamique de procédés à boues activées*. Thèse de doctorat. Toulouse: Génie des Procédés, INSA., 1999.
33. Press WH, Teukolsky SA, Vetterling WT, Flannery BP. Numerical recipes in C++. In: *The Art of Scientific Computing*. New York: Cambridge University Press; 2002:655–660.
34. Henze M, Gujer W, Mino T, van Loosdrecht MCM. *Activated sludge models ASM1, ASM2, ASM2d and ASM3*. UK: IWA publishing; 2000.
35. Bremer H, Dennis PP. Modulation of chemical composition and other parameters of the cell by growth rate. In: Neidhardt FC, Curtiss R, Ingraham JL, Lin ECC, Low KB, Magasanik B, Reznikoff WS, Riley M, Schaechter M, Umbarger HE, editors. *Escherichia coli and Salmonella, Cellular and Molecular Biology*. Washington: ASM Press; 1996:1553–1568.
36. Keener J, Nomura M. Regulation of ribosome synthesis. In: Neidhardt FC, Curtiss R, Ingraham JL, Lin ECC, Low KB, Magasanik B, Reznikoff WS, Riley M, Schaechter M, Umbarger HE, editors. *Escherichia coli and Salmonella, Cellular and Molecular Biology*. Washington: ASM Press, 1996:1417–1431.
37. Daigger GT, Grady CLP, Jr. An assessment of the role of physiological adaptation in the transient response of bacterial cultures. *Biotechnol Bioeng.* 1982;24:1427–1444.
38. Preiss J. Regulation of glycogen synthesis. In: Neidhardt FC, Curtiss R, Ingraham JL, Lin EC. C, Low KB, Magasanik B, Reznikoff WS, Riley M, Schaechter M, Umbarger HE, editors. *Escherichia coli and Salmonella, Cellular and Molecular Biology*. Washington: ASM Press; 1996:1015–1024.
39. Harper WF, Jenkins D. The effect of an initial anaerobic zone on the nutrient requirements of activated sludge. *Wat Environ Res.* 2003;75:216–224.
40. Liao JC, Hou SY, Chao YP. Pathway analysis, engineering, and physiological considerations for redirecting central metabolism. *Biotechnol Bioeng.* 1996;52:129–140.
41. Wolfe AJ. The acetate switch. *Microbiol Mol Biol Rev.* 2005;69:12–50.
42. Death A, Ferenci T. Between feast and famine: Endogenous inducer synthesis in the adaptation of *Escherichia coli* to growth with limiting carbohydrates. *J Bacteriol.* 1994;176:5101–5107.
43. Chen R, Yap WMGJ, Postma PW, Baley JE. Comparative studies of *Escherichia coli* strains using different glucose uptake systems: Metabolism and Energetics. *Biotechnol Bioeng.* 1997;56:583–590.
44. Gupta S, Pilyugin SS, Narang A. The dynamics of single-substrate continuous cultures: The role of ribosomes. *J Theoret Biol.* 2005;232:467–490.
45. Masson CA, Hamer, G, Bryers JD. The death and lysis of microorganisms in environmental processes. *FEMS Microbiol. Rev.* 1986;39:373–401.
46. van den Berg HA. A generic view of classic microbial growth models. *Acta Biotheor.* 1998;46:117–130.
47. Gerdes K. Toxin-antitoxin modules may regulate synthesis of macromolecules during nutritional stress. *J Bacteriol.* 2000;182:561–572.
48. Hochman A. Programmed cell death in prokaryotes. *Crit Rev Microbiol.* 1997;23:207–214.
49. Nyström T. To be or not to be: the ultimate decision of the growth-arrested bacteria cell. *FEMS Microbiol Rev.* 1998;21:283–290.
50. Yarmolinsky MB. Programmed cell death in bacterial populations. *Science.* 1995;267:836–837.
51. Mikkola R, Kurland, CG. Is there a unique ribosome phenotype for naturally occurring *Escherichia coli*? *Biochimie.* 1991;73:1061–1066.
52. Baloo S, Ramkrishna D. Metabolic regulation in bacterial continuous cultures: 1. *Biotechnol. Bioeng.* 1991;38:1337–1352.
53. Beun JJ, Paletta F, van Loosdrecht MCM, Heijnen JJ. Stoichiometry of poly- $\beta$ -hydroxybutyrate metabolism in aerobic, slow growing, activated sludge cultures. *Biotechnol Bioeng.* 2000;67:379–389.
54. Vanrolleghem PA, Spanjers H, Petersen B, Ginestet P, Takaks I. Estimating (combinations of) activated sludge model no. 1 parameters and components by respirometry. *Wat Sci Technol.* 1999;39:195–214.
55. Shoemaker J, Reeves GT, Gupta S, Pilyugin SS, Egli T, Narang A. The dynamics of single-substrate continuous cultures: The role of transport enzymes. *J Theoret Biol.* 2003;222:307–322.
56. Barker DJ, Stuckey DC. A review of soluble microbial products (SMP) in wastewater treatment systems. *Wat Res.* 1999;33:3063–3082.
57. Chang HT, Rittmann BE. Transient responses incorporating products formation. *J Environ Eng ASCE.* 1989;115:476–479.
58. Oehmen A, Lemos PC, Carvalho G, Yuan Z, Keller J, Blackall LL, Reis M. Advances in enhanced biological phosphorus removal: from micro to macro scale. *Wat Res.* 2007;41:2271–2300.

## Appendix

Table A1. List of Variables

Symbol	Definition
$S_O$	Soluble oxygen (mg COD/L)
$S_S$	Soluble substrate (mg COD/L)
$S_{MP}$	Soluble microbial products (mg COD/L)
$S_{NH}$	Ammonia (mg N/L)
$B_S$	Intracellular substrate (mg COD/L)
$B_{STO}$	Storage material (mg COD/L)
$B_P$	Intracellular precursors (mg COD/L)
$X_H$	Heterotrophic biomass (mg COD/L)
$X_{ii}$	Inert suspended organic matter (mg COD/L)
$B_{PSS}$	Growth enzyme (ribosome) (mg/L)
$E_{STO}$	Storage enzyme (mg/L)
$E_{Bsha}$	High affinity uptake enzyme of soluble substrate (mg/L)
$E_{Bsla}$	Low affinity uptake enzyme of soluble substrate (mg/L)
$E_{BS(SMP)}$	Uptake enzyme of soluble microbial products (mg/L)

Table A2. List of Parameters

Symbol	Definition	Value
$\mu_{max}^{int}$	Intrinsic value of growth rate ( $d^{-1}$ )	15
$\beta_{XH}$	Decay rate of biomass ( $d^{-1}$ )	0.09
$k_{BP}^{max}$	Synthesis rate of precursors ( $d^{-1}$ )	0.084
$\beta_{BP}$	Decay rate of precursors ( $d^{-1}$ )	0.9
$kr_{Bs}^{max}$	Release rate of soluble material ( $d^{-1}$ )	3 (88) <sup>#</sup>
$k_{Bsha}^{max}$	Specific activity of substrate uptake enzyme with high affinity ( $d^{-1}$ )	1
$k_{Bsla}^{max}$	Specific activity of substrate uptake enzyme with low affinity ( $d^{-1}$ )	95
$k_{Bsto}^{max}$	Specific activity of storage enzyme ( $d^{-1}$ )	35
$\delta k_{Bsto}^{max}$	Specific activity of hydrolysis enzyme of stored material ( $d^{-1}$ )	1
$k_{BSMP}^{max}$	Specific activity of SMP uptake enzyme ( $d^{-1}$ )	1
$\alpha E_{Bsha}$	Increase rate of substrate uptake enzyme with high affinity ( $mg*mg\ COD^{-1}*d^{-1}$ )	1.5
$\alpha E_{Bsla}$	Increase rate of substrate uptake enzyme with low affinity ( $mg*mg\ COD^{-1}*d^{-1}$ )	20
$\alpha E_{BSMP}$	Increase rate of SMP uptake enzyme ( $mg*mg\ COD^{-1}*d^{-1}$ )	3
$\alpha E_{sto}$	Increase rate of storage enzyme ( $mg*mg\ COD^{-1}*d^{-1}$ )	1
$\beta_{Ebs}$	Decay rate of substrate uptake enzyme ( $d^{-1}$ )	0.06
$\beta_{EBSMP}$	Decay rate of SMP uptake enzyme ( $d^{-1}$ )	0.06
$b_{PSS}$	Decay rate of $B_{PSS}$ ( $d^{-1}$ )	0.5
$\beta_{Esto}$	Decay rate of $E_{STO}$ ( $d^{-1}$ )	0.6

<sup>#</sup> Value used in the substrate pulses experiments (see discussion).

Table A3. List of Parameters

Symbol	Definition	Value
$K_{SMP}$	Soluble microbial products half saturation coefficient (mg COD/L)	40
$K_{Ssha}$	Soluble substrate half saturation coefficient for high affinity enzyme (mg COD/L)	0.40
$K_{Ssla}$	Soluble substrate half saturation coefficient for low affinity enzyme (mg COD/L)	20
$K_{NH}$	Ammonia half saturation coefficient (mg N/L)	2
$K_O$	Oxygen half saturation coefficient (mg /L)	0.20
$K_{Bs}$	Intracellular substrate half saturation coefficient (mg COD/(mg COD))	0.0004
$K_{BP}$	Intracellular precursors half saturation coefficient (mg COD/(mg COD))	6
$K_{STO}$	Storage material half saturation coefficient (mg COD/(mg COD))	0.6
$K_{ibs}$	Intracellular substrate inhibition coefficient for substrate uptake process (mg COD/(mg COD))	0.01
$K_{bsof}$	Intracellular substrate half saturation coefficient for the SMP production (mg COD/(mg COD))	0.0005
$K_{isto}$	Intracellular substrate inhibition coefficient for hydrolysis enzyme of storage material (mg COD/(mg COD))	5

Table A4. List of Parameters

Symbol	Definition	Value
$f_{PSS}$	PSS fraction in active biomass (g/g COD)	0.68
$Y_{BS}$	Yield of intracellular substrate on soluble substrate (g/g)	0.88
$Y_{BSMP}$	Yield of intracellular substrate on soluble microbial products (g/g)	0.8
$Y_H$	Heterotrophic yield on intracellular substrate (g/g)	0.66
$f_{STO}^{max}$	Maximal fraction of storage material (g/g)	1 (7) <sup>#</sup>
$i_{nx}$	Nitrogen fraction of active biomass (g N/g COD)	0.068
$f_u$	Fraction of biomass leading to particulate products (g/g)	0.20

<sup>#</sup> Value used in the substrate pulses experiments (see discussion).